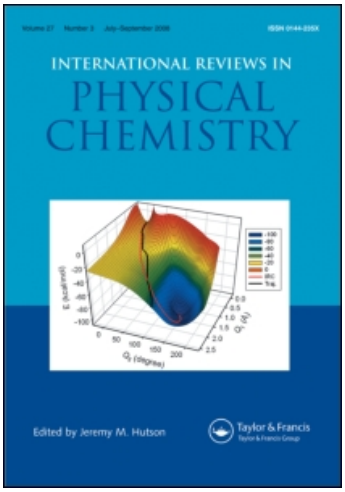

International Reviews in Physical Chemistry
Publication details, including instructions for authors and subscription information:
http://www.informaworld.com/smpp/title~content=t713724383

On the dynamics of chemical reactions of negative ions

Jochen Mikosch[a]; Matthias Weidemüller[b]; Roland Wester[c]
[a] National Research Council of Canada, Steacie Institute for Molecular Sciences, Ottawa, Ontario K1A OR6, Canada [b] Physikalisches Institut, Universität Heidelberg, 69120 Heidelberg, Germany [c] Physikalisches Institut, Universität Freiburg, 79104 Freiburg, Germany

Online publication date: 19 November 2010

To cite this Article Mikosch, Jochen , Weidemüller, Matthias and Wester, Roland(2010) 'On the dynamics of chemical reactions of negative ions', International Reviews in Physical Chemistry, 29: 4, 589 — 617
To link to this Article: DOI: 10.1080/0144235X.2010.519504
URL: http://dx.doi.org/10.1080/0144235X.2010.519504

International Reviews in Physical Chemistry
Vol. 29, No. 4, October–December 2010, 589–617

Taylor & Francis
Taylor & Francis Group

On the dynamics of chemical reactions of negative ions

Jochen Mikosch[a], Matthias Weidemüller[b] and Roland Wester[c]*

[a]*National Research Council of Canada, Steacie Institute for Molecular Sciences, 100 Sussex Drive, Ottawa, Ontario K1A OR6, Canada;* [b]*Physikalisches Institut, Universität Heidelberg, Philosophenweg 12, 69120 Heidelberg, Germany;* [c]*Physikalisches Institut, Universität Freiburg, Hermann-Herder-Straße 3, 79104 Freiburg, Germany*

(*Received 13 June 2010; final version received 20 August 2010*)

This review discusses the dynamics of negative ion reactions with neutral molecules in the gas phase. Most anion–molecule reactions proceed via a qualitatively different interaction potential than cationic or neutral reactions. It has been and still is the goal of many experiments to understand these reaction dynamics and the different reaction mechanisms they lead to. We will show how rate coefficients and cross-sections for anion–molecule reactions are measured and interpreted to yield information on the underlying dynamics. We will also present more detailed approaches that study either the transient reaction complex or the energy- and angle-resolved scattering of negative ions with neutral molecules. With the help of these different techniques many aspects of anion–molecule reaction dynamics have been unravelled in the last few years. However, we are still far from a complete understanding of the complex molecular interplay that is at work during a negative ion reaction.

Keywords: negative ions; ion-molecule reactions; reaction rates; reaction dynamics; cold chemistry; time-resolved dynamics; crossed-beam imaging

Contents

*Corresponding author. Email: roland.wester@physik.uni-freiburg.de

ISSN 0144–235X print/ISSN 1366–591X online

DOI: 10.1080/0144235X.2010.519504
http://www.informaworld.com

1. Introduction

Questions about the nature of chemical reactions, why and how they proceed and how this can be used to form certain desired chemical products are already very old. In fact they are older than most other current research topics in atomic and molecular physics or physical chemistry. The efforts to answer these questions have led to numerous achievements over the centuries, starting perhaps with the revelation of the discrete atomic structure of matter, leading to the invention of chemical catalysis, and including the understanding of the quantum mechanical nature of the chemical bond. Several technological advances have fertilized experimental research on the dynamics of chemical reactions. Besides the development of versatile tunable laser sources, one notes supersonic single and crossed molecular beams [1], multi-dimensional momentum imaging and coincidence detection [2–4], ultrafast time-resolved spectroscopy [5], and, most recently, the preparation of cold and ultracold atoms and molecules [6,7].

Today the study of the reaction dynamics of molecules has advanced to precise quantum-state resolved scattering experiments in quantitative agreement with high-level scattering calculations – at least for reactive complexes that involve no more than four atoms. If more atoms contribute to a chemical reaction the dimensionality of the scattering process, i.e. the number of degrees of freedom, increases beyond what quantum scattering calculations can do on current computers. Furthermore a separation of the degrees of freedom into relevant and irrelevant ones is generally not possible. Also experiments are challenged by the growing complexity, because individual quantum states are increasingly difficult to separate in the initial as well as the final state of a scattering event. However, it is precisely this 'complexity limit' in chemical dynamics that is driving a lot of research, because one would like to understand the details of reactions that are of relevance in organic chemistry, in living cells, or in the Earth's atmosphere. In such many-atom reactions new phenomena may occur that lead to different reaction mechanisms than in triatomic reactions.

Within the large field of reaction dynamics an important division follows the electric charge of the collision partners that participate in the reaction. Besides the neutral–neutral reaction processes, the second largest class are ion–molecule reactions. The ion–neutral interaction is much stronger than the neutral–neutral van der Waals interaction and leads to qualitatively different behaviour. Ion–molecule reactions often have very high rate coefficients and are thus important when ions are present in an environment. These environments include discharge plasmas [8], combustion processes, the Earth's ionosphere

[9], and many other stellar and interstellar regions [10,11]. Also in the condensed phase, more specifically in liquid solutions, ion–molecule reactions are important. Reactions of ions have consequently been studied for almost as long as neutral–neutral reactions. They require, however, significantly different experimental techniques.

A large portion of the research on ion–molecule reactions is devoted to positively charged ions. In dilute plasmas, ionization by electron impact or by radiation will directly lead to the formation of cations and they should therefore play an important role there. Nevertheless, also negatively charged ions are important constituents of gas phase environments, for example in the lower ionosphere of the Earth. Here the negative charge density is mostly represented by atomic and molecular anions (such as O^-, O_2^-, OH^-, HCO_3^-, NO_2^- and their clusters with water molecules) and not by free electrons [9]. Similarly negative ions are omnipresent in liquid solutions and have a strong impact on reactions there. Furthermore, negative ions are precursors for solvated electrons in liquids, which are responsible for strong optical absorption and have been the subject of many studies.

In recent years negative ions have also been detected in other planetary atmospheres in our Solar System, such as the atmosphere of Saturn's satellite Titan, and they have been found in the interstellar medium, in the dark molecular cloud TMC−1, and in a circumstellar shell around the carbon-rich star IRC+10216 [12,13]. The understanding of the complex chemistry that leads to anions in these areas is still fragmentary. The questions here are not only related to the formation of the anions, but also whether they can add new formation pathways to the complex neutral molecules found in the interstellar medium, such as long unsaturated carbon chains or possibly polyaromatic hydrocarbon molecules.

The study of the reaction dynamics of anion–molecule reactions is the topic of this review. Comparisons with cation–molecule reactions will be made where appropriate. Chemical reactions of negative ions have been studied extensively for many decades. Several excellent reviews have appeared a few years ago on this topic [14–16]. Here, we will concentrate specifically on the reaction dynamics in contrast to the kinetics of anion–molecule reactions. 'Molecular reaction dynamics is the study of elementary processes [of molecular collisions] and the means of probing them, understanding them and controlling them.' [17]. In this sense we focus on processes where isolated molecules collide in a well-controlled reactive event with a negative ion. We give an overview of all the major experimental techniques that are used to study anion–molecule reaction dynamics. In particular, we include the recent experimental developments, on the one hand cryogenic ion traps, and on the other hand ion–molecule crossed-beam imaging, and show how they provide new insights.

Negative ions are also subject to spectroscopic studies in the infrared and optical range, using bound–bound absorption and bound–free photoelectron spectroscopy. This reveals the stability, i.e. the electron affinity of the neutral, as well as structural information about the anion. Since negative ions are today still challenging for quantum chemical calculations, due to the spatial extension of the wavefunction of the excess electron and its interaction with the atomic core, spectroscopy and detachment studies can provide benchmark data [4,18–22]. Photoelectron spectroscopy of negative ions can also reveal the energy level structure of the neutral system that is reached after photodetaching the excess electron. If the neutral system is not a bound molecule, but a reactive complex, such as for

the FH_2^- anion, one can even study neutral reactions near the transition state between reactants and products [23]. For more information on the spectroscopy of negative ions see [24–26].

This article will start with a few general considerations of anion–molecule collisions and reactions in the next section. Then we will discuss how measurements of integral cross-sections or total rate coefficients, respectively, are performed. They are carried out either at a given collision energy or a given sample temperature and can already be used to infer information on the underlying reaction dynamics. In the next section, experimental approaches are presented that allow the investigation of the transient reaction complex. Then in Section 5 experiments with crossed beams are described, which allow the determination of energy- and angle-differential cross-sections, under optimum conditions even quantum-state resolved. From these measurements a wealth of information about the collision and reaction dynamics can be extracted. In the final section some of the future directions for the study of anion–molecule reaction dynamics are highlighted.

2. Anion–molecule interactions

The understanding of the dynamics of an anion–molecule reaction starts with the description of the interaction potential, usually in the Born–Oppenheimer approximation. The long-range and short-range properties of the interaction potential are discussed in the following sections. The proper theoretical treatment of the dynamics of the colliding molecules and ions on the interaction potential is a quantum scattering calculation [27–29], which is usually, however, limited to a reduced set of dimensions by the computational effort. Alternatively, the atomic motion is treated with classical dynamics [30,31], which is generally a good assumption because of the small de Broglie wavelength of the atoms. In this case all dimensions can be included, but such effects as the zero-point motion, tunnelling through potential barriers or quantum scattering resonances can usually not be accounted for.

2.1. *Long-range and short-range potentials*

At large distances the force between an ion and a neutral molecule is determined by the electrostatic interaction potential of the ion with the induced, and possibly also permanent, electric dipole moment of the molecule:

$$V(R) = -\frac{q^2\alpha}{2R^4} - \frac{q\mu}{R^2}\cos\theta \tag{1}$$

where α is the orientationally averaged polarizability and μ is the permanent dipole moment of the neutral molecule. q is the charge of the colliding ion. In certain cases also the ion–quadrupole interaction and other higher order multipole terms need to be added.

If the molecule carries a permanent dipole moment its interaction with the charge, which scales as R^{-2}, typically dominates over the induced-dipole interaction, which scales as R^{-4}. However, at large relative separation the free rotation of the molecule leads to a vanishing time-averaged permanent dipole moment. At the largest interatomic distances the ion-induced dipole interaction is therefore most important, which is always attractive. Once the interaction potential then becomes comparable to the rotational energy 'locking'

of the permanent molecular dipole to the incoming ion may occur and will thereby enhance the attractive interaction.

At short distances the electronic wavefunctions of the ion and the molecule interact. Determining the short-range interaction potential therefore requires solving the Schrödinger equation for the collision system. This is often particularly difficult for negative ions, because the excess electron is so delocalized that a large basis set is required in the numerical solution of the Schrödinger equation. However, it works as an advantage that many negative ions of interest are 'closed-shell' systems with a spin singlet configuration of the electronic wavefunction, because these are the most stable negative ions with respect to electron detachment. As a consequence, only a single Born–Oppenheimer potential hypersurface governs the reactions of such negative ions with closed-shell neutral molecules.

For many negative ion–neutral collision systems a repulsive potential is obtained at very short range. This may be attributed to the electron–electron repulsion by electrostatic forces and the Pauli exclusion principle. Together with the strong attractive interaction this leads to potential energy landscapes with two characteristic minima along the reaction coordinate, as shown in Figure 1. The path along the reaction coordinate is defined as the path of minimum potential energy that connects the reactants with the products. The potential energy minima typically lie several hundred meV below the asymptotic energies. Consequently, substantial short-range energy barriers may have negative transition state energies, as shown in Figure 1. But even if the transition state energy is negative, it can have a profound influence on the reactivity as we will see in the next paragraph. This is in contrasts to most reactions of cations, because there is usually no, or at least no substantial, short-range barrier.

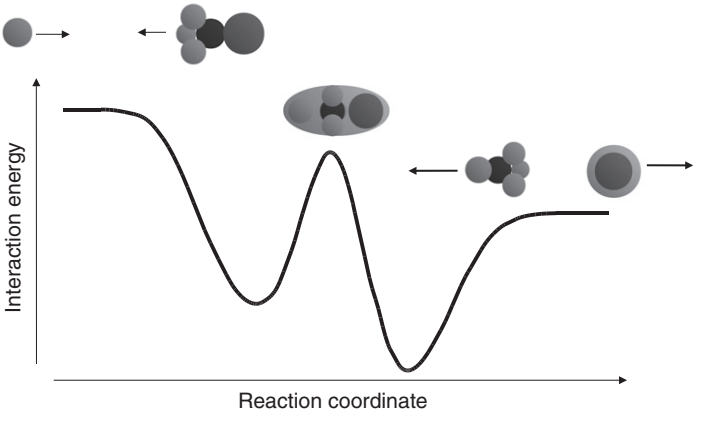

Figure 1. Schematic view of the Born–Oppenheimer potential of an anion–molecule nucleophilic substitution reaction along the reaction path. This path is defined as the lowest-energy trajectory across the Born–Oppenheimer hypersurface that connects the reactants with the products. The presented potential exhibits two minima and an intermediate reaction barrier between them, which is a typical configuration for many anion–neutral reactions. Often the barrier is found below the energy of one of the asymptotes.

2.2. *Capture model*

The kinetics of a chemical reaction, which describes the rate at which products are formed as a function of time, is usually characterized by the reaction rate coefficient. For a bimolecular reaction that occurs in a collision of two species the second-order rate equation

$$\frac{\mathrm{d}n_{\mathrm{product}}}{\mathrm{d}t} = k n_{\mathrm{reactant1}}\, n_{\mathrm{reactant2}} \tag{2}$$

describes the time-dependent increase of the product particle density n_{product} for given reactant densities $n_{\mathrm{reactant1,2}}$. This equation is typically applied to thermal ensembles. The second-order rate coefficient, k, is then dependent on the absolute temperature, T. It is related to the scattering cross-section, $\sigma(v_{\mathrm{rel}})$, for the individual collision events, which depends on the relative velocity, by the thermal average

$$k = \langle \sigma(v_{\mathrm{rel}}) v_{\mathrm{rel}} \rangle_T = \int_0^\infty \sigma(v_{\mathrm{rel}})\, p_T(v_{\mathrm{rel}}) v_{\mathrm{rel}}\, \mathrm{d}v_{\mathrm{rel}} \tag{3}$$

where $p_T(v_{\mathrm{rel}})$ is the thermal probability distribution for the relative velocities at absolute temperature T.

The standard model to estimate collision rates of ions with neutral atoms or molecules is the Langevin or capture model [17]. The assumption of this model is that a collision occurs with 100% probability if the two collision partners come closer to each other than a critical distance. Only the longest-range attractive interaction, the ion-induced dipole potential (the first term in Equation 1), and the repulsive centrifugal potential are taken into account. This critical distance is then given by the location of the maximum of the centrifugal barrier. The largest impact parameter for a scattering trajectory that reaches this critical distance and can surmount the centrifugal barrier determines the scattering cross-section. For larger impact parameters the ion–neutral interaction is neglected. With an additional thermal averaging, this assumption yields the Langevin rate coefficient (in SI units)

$$k = \frac{|q|}{2\epsilon_0}\sqrt{\frac{\alpha}{m_{\mathrm{r}}}}, \tag{4}$$

which turns out to be temperature independent. α is again the orientation-averaged polarizability of the neutral molecule while m_{r} denotes the reduced mass of the two-body system (q is the ion charge and ϵ_0 the electric constant). Typical Langevin rate coefficients range between $5 \times 10^{10}\,\mathrm{cm^3/s}$ and $5 \times 10^{9}\,\mathrm{cm^3/s}$.

A correction to the Langevin rate coefficient has to be introduced if the neutral target carries a permanent dipole moment μ. Then the second term in Equation (1) needs to be included. The 'average dipole orientation' approach [32] introduced an effective 'dipole locking constant' from which an improved collision rate coefficient was derived. In a more accurate approach, the rate coefficient for ion–polar-molecule collisions is obtained from a series of classical trajectories that are calculated to numerical precision for the exact interaction potential. The parameterization of these trajectories leads to a pre-factor $K(T) > 1$ to the Langevin rate constant in Equation (4), which is a function of μ and α [33–35]. As an effect, the ion–polar-molecule capture rate coefficient is typically a factor of 2–4 larger than the prediction for the Langevin rate coefficient.

3. Dynamics inferred from kinetics

The Langevin rate constant has proven to be extremely valuable as a guideline and often describes fairly accurately measured reaction rates for cations with non-polar neutral molecules [36]. When the observed rate coefficient for an ion–molecule reaction is smaller than the capture rate coefficient, which occurs when the reaction probability after crossing the centrifugal barrier is smaller than 100%, temperature- or energy-dependent rate coefficient measurements can be used to infer information about the reaction dynamics at short internuclear separation.

In the following sections this approach will be illustrated with several studies from recent years. Most major experimental techniques that are used for these studies, drift and flow tubes, guided ion beams, free jet expansions and low-temperature ion traps, will be discussed. Ion cyclotron resonance experiments and high-pressure mass spectrometry (see e.g. [15]), however, are beyond the scope of this article and will not be covered here.

3.1. *Reaction rate coefficients from drift tubes*

Flow and drift tubes have been the classic workhorses for the acquisition of ion–molecule reaction rate coefficients. They have produced a wealth of atmospherically and astrophysically relevant data over the almost 50 years of their existence [37–41]. Today they are found in many different variants, e.g. [42–45]. These instruments usually operate at room temperature, but may also be heated up to more than 1000 K or cooled down to near liquid nitrogen temperatures (77 K). Ions are created typically by electron impact, eventually chemically transformed and mass selected, and then injected into a constant flow of buffer gas of several m/s velocity. The pressure of this buffer gas, which is usually helium, is of the order of a few millibars. Consequently, the mean free path of the ions is smaller than the dimension of the tube and the flowing buffer gas transports the thermalized ions downstream through the flow tube. A distance away from the ion source, neutral reactant gas is injected. Due to reactions of the ions with the neutral gas their density decreases with flow time, which now corresponds to the flow distance. At the same time, product ions are generated. By sampling ion yield and composition with a quadrupole mass spectrometer as a function of flow distance, absolute reaction rate coefficients can be extracted. Their temperature dependence may be obtained by heating or cooling the buffer gas inlet and flow section. An electric field gradient may be applied along the flow section turning the flow tube into a drift tube. This allows studies at elevated kinetic energy rather than temperature.

The rate coefficient gives a first hint of the dynamics of an ion–molecule reaction. Barrier-less proton transfer reactions usually exhibit large rate coefficients in accordance with the capture model [46]. In contrast, many anion–molecule reactions feature orders of magnitude lower rate coefficients, pointing to dynamical bottlenecks and intermediate barriers on the potential energy hypersurface. Chemically versatile flow and drift tubes are well suited to study the effects of chemical substitution on the rate coefficient [47]. Different reaction mechanisms leading to the same (ionic) products may be distinguished by studying kinetic isotope effects [48,49]. More direct insight into the dynamics can be obtained from a temperature-dependent flow tube measurement of the rate coefficient [50,51]. Moreover, in drift tubes internal and translational degrees of freedom of the reaction partners are decoupled and can be separately controlled. This allows us to

investigate how the reaction rate changes if the same amount of energy is provided in different forms, challenging the statistical model of the reaction dynamics [52].

Probably the most important type of anion–molecule reaction that has been studied up to now is the nucleophilic substitution (S_N2) reaction [53,54]:

$$X^- + CH_3Y \rightarrow Y^- + CH_3X, \tag{5}$$

where X and Y can be anything from simple halogen atoms to large macromolecular systems. The assumption of statistical energy redistribution was a matter of fierce debate in the 1990s in the framework of S_N2 reactions. A variable temperature flow tube study had shown that the $Cl^- + CH_3Br$ reaction rate is strongly dependent on the relative translational energy, while being at the same time insensitive to the internal temperature of the reactants [52]. Such behaviour is in clear contradiction with the statistical assumption of rapid randomization of all available energy in the $[Cl\cdots CH_3Br]^-$ entrance channel complex. This observation prompted a large number of theoretical studies, which uncovered a dynamical bottleneck for energy transfer between internal modes of CH_3Br and the intermolecular low-frequency modes [53].

In a recent application of an ion flow tube instrument, the competition between nucleophilic substitution (S_N2) and base-induced elimination (E2) was investigated via chemical substitution and the deuterium kinetic isotope effect [49,55]. Villano *et al.* studied the reaction of BrO^- and ClO^- with methyl chloride (CH_3Cl) and its partially and fully methylated form CXYZCl (where X, Y, Z can be either H or CH_3). The S_N2 and E2 mechanisms lead to the same ionic reaction product, a challenge for all experiments, which rely on charged particle detection. The authors used the fact that deuteration of the neutral reactant changes the rate of the reaction. The deuterium kinetic isotope effect is defined as the ratio of the perprotio to perdeuterio rate coefficients ($KIE = k_H/k_D$). Whereas for CH_3Cl an inverse KIE was determined (i.e. $KIE < 1$), the KIE was found to become increasingly more normal ($KIE > 1$) as the extent of methyl-substitution in the neutral reactant is increased. For the reaction of BrO^- with the fully methylated neutral species, a factor of about 3 larger reaction rate coefficient was measured for $(CH_3)_3CCl$ as compared to its deuterated form $(CD_3)_3CCl$. Villano *et al.* referred to a marked effect of deuteration on the vibrational dynamics near the respective transition states of the S_N2 and the E2 mechanism [56]. They argued that the E2 pathway is a minor channel for the small neutral reactant CH_3Cl, whereas it becomes gradually more important with increasing methylation of the neutral, which sterically hinders and finally impedes nucleophilic substitution.

The oxidation of the trichlorooxyphosphorus anion $POCl_3^-$, which occurs in combustion flames, has been recently studied by Kerkines *et al.* [51]. Despite its very low rate coefficient of only around $1 \times 10^{-14}\,cm^3/s$ (at 300 K), such oxidations can change the chemistry of flames due to the high abundance of O_2. The authors employed a turbulent ion flow tube, where orders of magnitude higher neutral gas densities can be applied as compared to the conventional laminar flow tubes [44]. They measured the rate coefficient over the range 300–626 K and found it to increase slowly with increasing temperature. An Arrhenius fit yielded an activation energy of 50 meV. Since the oxidation is exothermic by about 1.8 eV, the presence of an intermediate potential barrier was concluded. Examination of the reaction pathways at different levels of molecular orbital theory led to the proposal of a multistep reaction mechanism. It involves product formation via the transformation of the entrance channel ion-dipole complex into a

four-membered P···O–O···Cl ring transition state, the highest point on the potential energy surface.

The highest temperature studies of ion–molecule reactions under fully thermalized conditions have been undertaken in a high temperature flowing afterglow apparatus at up to 1800 K [41]. For an anion–molecule reaction, 1440 K has been reached for $CO_3^- + SO_2 \rightarrow SO_3^- + CO_2$ [57]. The main driving force for these technically challenging experiments is to model the chemical environment of the Earth's ionosphere and other planetary atmospheres at high altitude. However, these studies are also interesting from the reaction dynamics point of view. At these high temperatures even small molecules carry significant amounts of rotational and vibrational excitation. We can explored how energy supplied in different forms – translational or internal – affects the reaction rate. For the reaction of CO_3^- with SO_2, Miller *et al.* found by comparison with drift tube data that the total energy alone controls the reactivity [57]. They concluded that the independence of the rate coefficient on the form of energy implies that the reaction is governed by long lived intermediates in which energy equilibrates, even at very high temperatures.

3.2. *Integral cross-sections from guided ion beams*

Guided ion beam (GIB) studies are the method of choice for precise measurements of integral reaction cross-sections of ion–molecule reactions for collision energies of the millielectronvolt to the tens of electronvolt range. These measurements also allow for the determination of the opening and competition of different reactive channels in ion–molecule collisions [58]. Teloy and Gerlich introduced GIBs into gas-phase chemistry in pioneering experiments in Freiburg in the 1970s [59]. In this technique mass-selected ions are passed into a long radio-frequency (rf) multipole ion guide – typically an octupole – with a selected kinetic energy, controlled by the dc potential difference between the ion source and the ion guide. Importantly, the guiding multipole electric rf field contains the ions radially, while at the same time minimizing alteration of their kinetic energy. The latter is crucial to the technique and impedes the use of quadrupole rf fields: Micro-motion of the ions driven by the oscillating field results in energetic collisions with the buffer and reaction gas. These effects are referred to as radio-frequency heating and are minimized in a multipole rf field [60]. The created effective potential guides the ions through a scattering cell located at the centre of the long guide.

The neutral reaction partner is introduced into the scattering cell – which may be temperature-variable [61] – at a well characterized density. Ions collide with the neutrals as they pass through the scattering cell and undergo chemical reactions. Note that the multipole guide also contains the ionic reaction products. All ions are mass analysed when they reach the end of the guide, typically with a quadrupole mass selector. Counting the number of reactant and product ions allows one to determine absolute integral cross-sections for ion–molecule reactions and collision-induced dissociation. These measurements can be done as a function of the relative kinetic energy of the reactants over an extended range of energies from about 0.1 to hundreds of electronvolts. GIB measurements achieve high resolution since they ensure single collision conditions in contrast to drift tubes and employ better defined, narrow ion velocity distributions [62]. At the same time the range of relative collision energies is extended since ions are radially contained and cannot get lost by drifting to the walls of the tube. To further minimize the energy

spread of the reactants, sophisticated ion sources such as flow tubes and multipole traps are used [62–64].

The bulk of GIB studies have focused on positively charged ions. Negative ion chemistry has been investigated in particular by the group of Kent Ervin, with special emphasis on nucleophilic substitution. To uncover reaction dynamics and mechanisms, the group heavily employs *ab initio* calculations and density functional theory in the interpretation of their measurements. The high resolution of GIB measurements allows them to reveal the threshold behaviour of endoergic reactions [65] and of exothermic reactions, which feature an intermediate potential barrier [62]. The wide tunability of the relative collision energy enables studies of the opening and interplay of reaction mechanisms leading to different ionic products. Absolute integral cross-sections of competing nucleophilic substitution and abstraction reactions were obtained [66,67]. Collision-induced dissociation of anion–dipole complexes accesses the dynamics at the transition state [68]. In an advanced mode of operation, GIB experiments may be run in a pulsed manner and the dwell time of the ionic reaction products in the long guide may be used to analyse their axial kinetic energy distribution. This allows us, to some degree, to distinguish between forward and backward scattering for a more direct insight into ion–molecule reaction dynamics [63,69].

Haufler, Schlemmer and Gerlich carried out a pioneering GIB study for anions, investigating the fundamental molecular reaction $H^- + D_2 \rightarrow D^- + HD$ and its isotopic variant $D^- + H_2 \rightarrow H^- + HD$ [63]. Integral cross-sections have been obtained as a function of collision energy between 0.1 and 10 eV translational energy in the centre-of-mass frame. They show an onset at around 0.3 eV, a maximum at around 1 eV and a decrease at larger collision energies. Barriers of 350 and 330 meV were deduced for $H^- + D_2$ and $D^- + H_2$, respectively. The decrease of the cross-section was attributed to the competition with collisional electron detachment of the reactant anion. Interestingly, it was found that the integral cross-section of the heavy ion colliding with the light molecule is larger by a factor of 2, reaching 2.7 $Å^2$ at its maximum. Axial product time-of-flight distributions have been measured by recording arrival times and converted to differential cross-sections $d\sigma/dv_p$ (v_p denotes the velocity component of the products along the guide). Preferred forward scattering was found for low collision energies just above threshold. By variation of the depth of the effective potential via the rf amplitude, which probes the transversal velocity distribution, the authors concluded that internal excitation of the product molecule is not significant at these energies. Thus they were able to deconvolute $d\sigma/dv_p$ to obtain angle-differential cross-sections $d\sigma/d\theta$. These could be cross-calibrated against crossed-beam data [70] (see Section 5.1). The angle-differential cross-sections were found to be quite similar for the two variants of the reaction, despite the big isotope effect observed in the integral cross-section. The authors concluded that the region of the potential energy surface probed in the exit channel has to be similar and the increased reactivity of $D^- + H_2$ has to stem from dynamics in the entrance channel.

DeTuri *et al.* investigated the symmetric S_N2 reaction $Cl^- + CH_3Cl \rightarrow ClCH_3 + Cl^-$ [62] by isotopic labelling. For this system, a translational energy threshold of 2 eV had been determined 10 years before in a pioneering and well-recognized drift tube measurement by the Bierbaum group [71]. Based on that finding, anionic attack on the chlorine side of chloromethane ('front-side attack') had been proposed as the reaction mechanism (potential barrier 2.0 eV), and this has subsequently been backed by theoretical

studies [72,73]. In contrast, DeTuri *et al*. determined a translational energy threshold of 470 ± 160 meV in their GIB experiment. The authors argued that the previous measurement had been affected by the skewed reactant kinetic energy distribution in the drift tube as well as by collisions with its high-density helium buffer gas during the lifetime of the entrance channel complex. The adjusted threshold, however, energetically excludes front-side attack as the reaction mechanism. On the other hand, the conventional S_N2 back-side attack mechanism, with inversion of the carbon centre, features a potential barrier height of only around 120 meV, substantially lower than the threshold measured by DeTuri *et al*.

This puzzle prompted a lot of studies on the theoretical side. Quasiclassical trajectory simulations by the Hase group both on an analytical potential energy surface [74] and with the *ab initio* direct dynamics method [75] as well as reduced-dimensionality quantum dynamical calculations [76,77] were undertaken. It was confirmed that front-side attack is not the reaction mechanism and back-side attack prevails. However, in contrast to the conventional S_N2 mechanism, it was found that only a very small fraction of the reactive trajectories are indirect, with transient trapping in the ion-dipole wells. This is assigned to poor coupling of the provided translational excitation to internal degrees of molecular freedom. A direct pathway of product formation, on the other hand, seems to feature strict dynamical constraints for low collision energy such as a very restricted geometry of approach for passing over the minimum energy barrier.

The power of the GIB technique is nicely demonstrated in complementary cross-section studies of the exothermic S_N2 reaction $F^- + CH_3Cl$ and its counterpart, the endothermic reverse reaction $Cl^- + CH_3F$ [66,67]. The data from Angel and Ervin are reproduced in Figure 2(a) and (b). As can been seen, the measured reaction cross-sections range over an impressive dynamic range from more than 10^2 Å^2 down to 5×10^{-4} Å^2. The exothermic S_N2 reaction leading to Cl^- product formation is most efficient at the lowest centre-of-mass collision energies, while its cross-section decreases rapidly over the range 0.1–2 eV. The reason for this behaviour derives from the S_N2 reaction mechanism. A more impulsive collision allows for less alignment of the reaction partners along the back-side attack coordinate by their ion-dipole interaction, i.e. along the near collinear reaction path. Figure 2(b) shows that the endothermic S_N2 reaction leading to F^- product formation features an energy threshold as expected. Angel and Ervin determined a threshold energy of 1.88 eV, which is 0.54 eV in excess of the reaction endothermicity.

Inspecting the pseudo-collinear PES, the authors interpreted their finding in terms of the Polanyi rules [78]. An early transition state in the exothermic direction for the collinear reaction pathway renders translational energy efficient in promoting the reaction. This accounts for the high cross-section in excess of 100 Å^2 for low collision energies. After translational passage over the barrier trajectories need to pass the 'bend' along the reaction coordinate to form products. Hence much of the reactant translation is expected to be converted into excitation of the C–Cl stretch vibration of the product molecule. Microscopic reversibility suggests in turn that vibrational excitation of CH_3Cl is needed in the endothermic direction to efficiently pass the initial tight bend on the PES before surmounting the late transition state. Translational activation such as in the GIB experiment should hence be inefficient at promoting the endothermic reaction. This is in accordance with the finding of an excess barrier by Angel and Ervin and a low cross-section of maximal 0.6 Å^2. Figure 2 shows that at higher collision energies other reaction channels open up and compete with nucleophilic substitution. For the exothermic

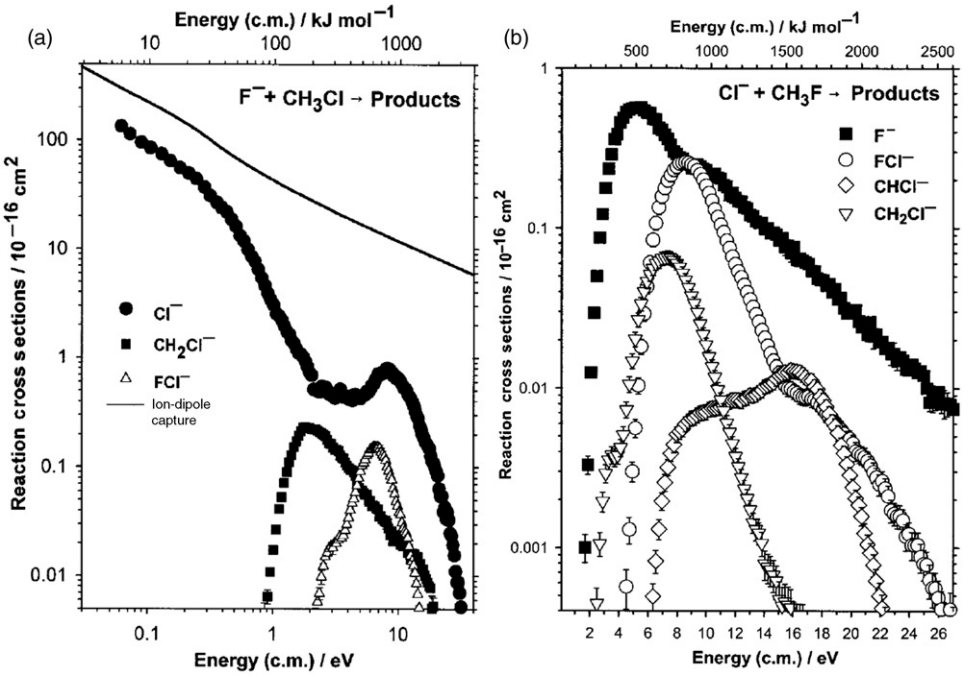

Figure 2. Absolute integral cross-section from a GIB study of $F^- + CH_3Cl$ (a) and the inverse reaction $Cl^- + CH_3F$ (b) for different product ions as a function of the relative collision energy. The calculated capture cross-section is shown as a solid line. Reprinted with permission from [66] and [67]. Copyright (2001), American Chemical Society.

direction (Figure 2a), both proton transfer and chlorine abstraction reactions were observed. At collision energies above 2 eV, the Cl^- cross-section was found to increase again. Dissociation of the CH_2Cl^- and FCl^- reaction products was proposed as an explanation. For the endothermic direction (Figure 2b), methylene and fluorine abstraction as well as a subsequent three-body dissociation were observed. Some of these reactions exhibit dual rising features. Reaction mechanisms have been proposed based on molecular structure calculations.

While GIB techniques are strong at determining integral reaction cross-sections, the very detailed and insightful study by Angel and Ervin also clearly shows their limitations. An experimental method is needed, which can provide more direct insight into the reaction dynamics and is capable of dissecting the partitioning of energy into translational and internal degrees of molecular freedom (see Section 5).

As first demonstrated by Gerlich [60] and already mentioned above, GIB methods can in fact provide to some degree more direct insight into the reaction dynamics by recording the arrival time of the product ions. Angel and Ervin applied this technique in a study of the exothermic S_N2 reaction $Cl^- + CH_3Br$ [69]. They reported the relative product velocity distribution along the axis of the ion guide for a series of relative collision energies between 0.1 and 4.0 eV. At 0.1 eV, the S_N2 product velocity was found to be symmetrically distributed around the centre of mass velocity and to agree well with the prediction of a statistical phase space theory (PST) model. This can be regarded as a strong sign that the

reaction is complex-mediated. At 0.25 eV, the velocity distribution becomes asymmetric with a preference for forward scattering of the CH_3Cl product. This shows that the reaction becomes more direct, with reactant interaction on a time-scale less than the rotational period of the complex. At 0.5 eV, backward scattering arises and becomes dominant above 1.0 eV. The authors interpreted this as the introduction of a direct rebound mechanism.

3.3. *Low-temperature reactions in jets and traps*

At lower and lower temperatures the dynamics of ion–molecule reactions become more sensitive to details of the interaction potential and to quantum dynamical effects such as tunnelling. Changes in the rate coefficients at low temperature also affect the abundance of ions in atmospheric and interstellar plasmas, which are often characterized by temperatures well below room temperature. This has raised substantial interest in low-temperature studies of ion–molecule reactions.

Very low temperatures, down to about 0.1 K, are reached in free jet supersonic flows employing adiabatic expansion [79]. However, the complex cooling process that is induced by the transient flow dynamics of an expanding free jet does lead to temperature disequilibria for the different molecular degrees of freedom and non-thermal rotational state distributions [80,81]. Despite these difficulties, supersonic jets have been used to study a few reactions of cations, produced by electron impact or laser ionization. Two examples are the study of vibrational quenching of $NO^+(v=1)$ via helium by complex formation below 3 K [82] and the reopening of the bimolecular $C_2H_3^+$ channel in the hydrogen transfer of H_2 to $C_2H_2^+$ for low temperatures, which is attributed to tunnelling of a collision complex through the reaction barrier [83]. An extension of this technique to negative ion reactions is not straightforward and has not been carried out up to now.

Uniform expansions from precisely designed Laval nozzles can overcome some of the difficulties of free jet flows by maintaining parallel streamlines at constant Mach number [79]. Constant high densities are reached at a fixed temperature in the travelling frame over the entire flow, which makes equilibration of the molecular degrees of freedom more likely. By terminating the supersonic expansion through parallelization of the streamlines in the nozzle, the exceedingly low temperatures of free expansions are unfortunately lost. This CRESU (a French acronym for Cinétique de Réaction en Ecoulement Supersonique) technique is applicable to negatively charged ions, created by dissociative electron attachment in the isentropic flow.

CRESU was employed by Le Garrec *et al.* to study the S_N2 reaction $Cl^- + CH_3Br$ from 180 down to 23 K [84]. Combining their results with previous measurements obtained from other experimental techniques, the authors demonstrated a dramatic increase in the rate coefficient by a factor of 400 upon reduction of the temperature from 500 to 23 K. A quantum scattering method, the 'rotating bond approximation', has been employed in this work. It was found that at the lowest temperatures the reaction follows the potential energy profile with no activation energy present. The excitation of intermolecular bending modes of the transition state then induces an activation barrier for increasing temperature.

With the exploration of radio-frequency heating in guided ion beams, it became clear that for efficient cooling and complete thermalization of molecular ions with a buffer gas, trapping in a quasi-field–free environment is indispensable [60]. Gerlich pioneered the

development of cryogenic storage devices based on electric multipole fields, which are capable of cooling molecular ions to a few kelvin in all degrees of molecular freedom. The most popular design is the 22-pole ion trap [85], which is nowadays used in a wide range of applications [86].

In such a temperature-variable 22-pole ion trap, the lowest temperature for an anion–molecule reaction up to now has been achieved in a recent experiment in our group [87]. The specific system under investigation was the proton transfer reaction to the negatively charged amide ion

$$NH_2^- + H_2 \rightarrow NH_3 + H^-. \quad (6)$$

For this reaction a room temperature reaction probability, given by the ratio of the measured rate coefficient to the calculated Langevin rate coefficient, of about 2% had been found many years ago [88]. Thus, in 98% of the collision events the reactants are reproduced and no products are being formed. This occurs despite the fact that the reaction is exothermic and also the intermediate potential barrier lies below the energy of the entrance channel. It shows that for this reaction the reaction dynamics at short range are very important.

At lower temperatures the probability for reaction (6) increases strongly [87]. The data are shown in the right panel of Figure 3. At 20 K the probability has increased by a factor of 6. This increase is a manifestation of the complex-mediated reaction dynamics [89]: the intermediate NH_4^- complex, which is transiently formed during a collision that surmounts the centrifugal barrier, has a longer lifetime with respect to decay back to reactants at lower temperatures, because the number of available decay channels decreases. The probability of crossing the intermediate potential barrier and forming products, however, remains approximately constant. Therefore the overall probability to react increases. The observed decrease of the reaction probability for temperatures lower than 20 K

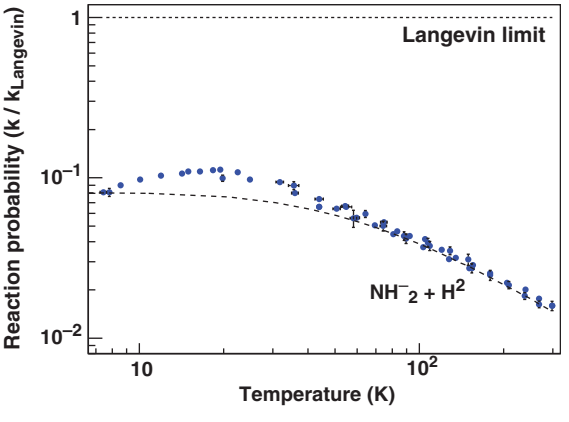

Figure 3. [Colour online] Reaction probability, given by the ratio of the measured rate coefficient and the constant Langevin rate coefficient, for the reaction of NH_2^- with H_2 (Equation 6) as a function of temperature [87]. The data show that the probability for reaction increases with decreasing temperature but stays well below the Langevin limit. Below 20 K the data show an unexpected decrease of the reaction probability that cannot be explained by a classical statistical model (dashed line).

(see Figure 3) cannot be explained within the classical dynamics picture of a complex-mediated reaction mechanism. Instead it is expected to represent a signature of quantum mechanical reaction dynamics, i.e. the influence of the wave nature of the interacting atoms and the resulting non-continuous energy level spectrum of the reaction complex, in low-temperature ion–molecule reactions.

4. Probing the collision complex

In the following section we discuss experiments that investigate the transient complex that the reactants form along the path to reaction products. Experimentally, this is either achieved by analysing ternary, complex-forming reactions, by studying unimolecular decay of anion–molecule compounds or by applying direct time-resolved spectroscopy, as detailed below.

4.1. *Three-body association and dissociation of reaction intermediates*

Average lifetimes of transient entrance channel complexes formed upon collision of the reaction partners can be determined indirectly from ternary rate coefficients for their formation and collisional stabilization. For reactions of cations with neutral molecules, the extraction of complex lifetimes from ternary association has a long history using flow and drift tubes at high pressure. For reactions of anions, work has focused on the symmetric S_N2 reaction $Cl^- + CH_3Cl$, specifically the formation and unimolecular decay time of the metastable $[Cl^- \cdots CH_3Cl]^*$ entrance channel complex [90,91].

Ternary association is studied in a thermal environment, where the density of the neutral reaction partner and a buffer gas is well defined and controllable. It can be understood as a two-step process:

$$Cl^- + CH_3Cl \underset{k_\Gamma}{\overset{k_f n_{CH_3Cl}}{\rightleftharpoons}} [Cl^- \cdots CH_3Cl]^* \xrightarrow{k_s n'} [Cl^- \cdots CH_3Cl]. \quad (7)$$

In the first step collisions of the reactants Cl^- and CH_3Cl form the metastable ion-dipole complex under investigation, where the relative kinetic energy is transiently transferred into internal energy. The complex is highly excited with respect to its ground state and decays back to reactants with the unimolecular rate k_Γ. Stabilization of the complex can occur in a second step if a third particle impact removes more internal excitation from the complex than the initial relative translational and internal energy of its constituents. This is only a small fraction of its internal excitation given the binding energy of ground state $[Cl^- \cdots CH_3Cl]$ of about 450 meV with respect to the asymptote. In subsequent collisions the internal energy is thermalized with the environment. Re-excitation of the complex above the asymptote for dissociation is then strongly suppressed by the Boltzmann factor.

Conditions are arranged such that the stabilization step occurs with a high probability by the buffer gas, which is provided in large excess as compared to the reaction partners. At the same time, the low-pressure limit of the steady state approximation has to be valid, which practically means that it has to be ensured that stabilization of the complex is a rare event. Then the rates for the association and stabilization step in (7) are well defined and

the overall rate of $[Cl^- \cdots CH_3Cl]$ formation is $R = k_3 n_{CH_3Cl} n$, where k_3 is the ternary rate coefficient $k_3 = k_f k_s / k_\Gamma$. The ternary rate coefficient is experimentally determined by measuring R as a function of the densities of the reactant (n_{CH_3Cl}) and the buffer gas (n). The rate coefficients k_f and k_s describe barrier-free ion–molecule reactions; the method relies on the assumption that these rate coefficients are very close to the capture-limited values. With this, the unimolecular dissociation rate can be extracted, the inverse of which is the average lifetime of the excited collision complex $[Cl^- \cdots CH_3Cl]^*$.

Li *et al.* studied ternary association with high pressure mass spectrometry and obtained an average lifetime of 12–16 ps for $[Cl^- \cdots CH_3Cl]^*$ at a fixed temperature of 296 K [90] (see also [91]). In a recent experiment in our group, a 22-pole radio-frequency ion trap has been employed, which provides the advantage of temperature variability and long interaction times [91]. This allows us to study the complex lifetime as a function of reactant collision temperature down to 150 K, at which point the vapour pressure of the neutral reactant becomes too low to be bearable. We have found a strong inverse temperature dependence of the average lifetime of the transient $[Cl^- \cdots CH_3Cl]^*$ complex in disagreement with a simple statistical model. Longer lifetimes of the entrance channel complex at lower temperatures give S_N2 reaction systems more time to exploit the available phase space, randomize energy, cross the central reaction barrier and finally form reaction products. This substantiates further that enhanced lifetimes of the transient entrance channel complex are likely to underlie the strong inverse temperature dependence of rate coefficients for exothermic S_N2 reactions with a submerged barrier.

Unimolecular dissociation of the metastable reactant complex into products

$$[X^- \cdots CH_3Y]^* \rightarrow Y^- + CH_3X \tag{8}$$

was studied in a series of experiments on asymmetric S_N2 reactions by the Bowers group [92–94]. Since entrance channel complexes were prepared, the formation of products involves at least one crossing of the intermediate reaction barrier. Relative kinetic energy distributions for the released products were recorded by means of ion kinetic energy spectroscopy. The measurements were compared to statistical phase space theory. Somewhat controversial in these decomposition experiments is the initial state of the metastable reactant complexes under investigation. They have to have sufficient lifetime to survive transport from the high-pressure ion source to the field-free high-vacuum region of the employed mass spectrometer and still undergo unimolecular dissociation. This renders partial collisional stabilization in the ion source likely (see also [50]). The kinetic energy release distributions for the investigated S_N2 reactions all peak at zero relative kinetic energy of the products and rapidly decrease for increasing energy. Interestingly, despite the long complex lifetimes the experimental distributions are much narrower than the calculated ones based on phase space theory. This means that less energy is partitioned to relative translation of the dissociating products than predicted for a statistical redistribution of energy. The phase space calculation was brought into agreement with the experimental results only if a significant amount of energy was made unavailable for energy redistribution.

This effect remains if partial collisional stabilization is taken into account. The energy missing in translation has to be trapped in internal degrees of freedom of the reaction products. The authors argued that significant rotational excitation is not present and that

hence the neutral reaction product has to be vibrationally hot. Surprisingly, the same result was found for 'simple' S_N2 reactions of methylhalides [93] as well as for S_N2 reactions involving reaction partners with many more internal degrees of freedom [94]. While for the methylhalide reactions this observation is in agreement with classical trajectory studies [95], it challenges the notion that statistical theories become valid for more complex S_N2 reactions with extended complex lifetimes, whereas non-statistical dynamics is restricted to small or highly energized systems with short complex lifetimes on the order of tens of picoseconds [53,96]. For extended complex lifetimes, it was speculated that tunnelling through the central barrier might be an alternative way of product formation, leading to a reduced effective barrier height [50].

Dissociation of reaction complexes is ideally studied upon state-specific excitation of an initially cold complex. For $Cl^- \cdots CH_3Br$ it was found that excitation of high-frequency intramolecular vibrations in the CH_3Br moiety by a CO_2 laser leads exclusively to the product formation $Br^- + CH_3Cl$ [97]. This was predicted for this system by classical trajectory calculations from Hase and coworkers [95], which demonstrated an enhancement of central barrier crossing upon selective excitation. Similarly, excitation of the doubly degenerate C–H stretch modes in the same complex induces central barrier crossing and the formation of Br^- products [98]. Craig *et al.* created the S_N2 intermediate $[CF_3CO_2CH_3 \cdots Cl^-]^*$ in a highly vibrationally excited state by means of a precursor exothermic association reaction [99]. This resulted in an at least four-fold enhancement of the branching ratio for the S_N2 reaction pathway as compared to unexcited complexes. The observation is in disagreement with statistical RRKM calculations and was interpreted as a manifestation of a bottleneck for energy transfer between intra- and intermolecular modes on the time-scale of the complex lifetime [30].

4.2. *Time-resolved photoelectron spectroscopy*

Chemical reactions involve the nuclear motion from reactants to products as well as the coupled structural and energetic transformation of molecular orbitals. Ultrafast laser pulses allow us to follow half-reactions in real time by photoinitiating the dissociation of a transition state and probing the evolution to products with a second photon in a pump–probe experiment [100,101]. In time-resolved photoelectron spectroscopy (TRPES) the probe laser generates free electrons by photoionization or photodetachment, whose kinetic energy and eventually angular distribution is measured. Since TRPES is sensitive to both the electronic configurations and the vibrational dynamics, it has been a particularly successful tool for real-time insight into molecular photodynamics (see the recent reviews [102–104]).

In pioneering TRPES studies of negative ions, Neumark and coworkers time-resolved the photodissociation of the I_2^- anion [105,106]. An ultrashort laser pulse at 780 nm pumps ground state I_2^- ($X^2\Sigma_u^+$) to the first excited electronic state ($A'\ ^2\Pi_{g,1/2}$). Following this excitation, I_2^- dissociates into ground state products $I^- + I(^2P_{3/2})$ with a 0.6 eV kinetic energy release. At variable time delay with respect to photoinitiation an ultrashort probe pulse is employed, which produces a photoelectron spectrum (PES). For a 260 nm probe wavelength, two photoelectron bands are observed, which asymptotically correspond to photodetachment of the I^- photoreaction product. For short pump–probe delays, the photoelectron bands shift to smaller kinetic energy for increasing delay, while at the same

time their width narrows (see also [4]). This effect was attributed to the change in character of the orbital from which the photoelectron is derived. By tracing the transition from the molecular to atomic orbital, the PES reveals that the dissociation is complete within the first 320 fs after photoinitiation. Following dissociation, a subtle shift of the photoelectron kinetic energy in the opposite direction is observed, which continues for another 400 fs. This behaviour was assigned to the interaction of the separating fragments, in particular the polarization-induced charge-dipole attraction between the anion and the neutral atom. It corresponds to a shallow well on the long-range part of the potential surface, which was characterized in the TRPES experiment and determined to be 17 meV deep [106]. Measured photoelectron angular distributions reveal that the localization of the excess charge on one of the atoms is only complete after about 800 fs [107]. The observed dynamics in the exit channel of I_2^- photodissociation becomes upon time-reversal entrance channel dynamics for an $I^- + I$ collision.

Mabbs *et al.* [4,108] extended this work to the related system IBr^-. Here excitation at 780 nm – to the lowest optically bright excited electronic state – correlates to the second lowest product channel, $I^- + Br(^2P_{3/2})$. Again, a well is found in the long-range part of the potential, but compared to I_2^- it is about 60 meV deeper. Based on the result of a classical trajectory calculation, the authors transformed the time axis to the intermolecular distance R – thus providing an 'image' of the potential as a function of the reaction coordinate. Sanford *et al.* [109] showed that for the same photoexcitation the presence of a single solvent molecule introduces a new product channel, the formation of $I + Br^-$. Using TRPES, Sheps *et al.* traced this back to a non-adiabatic transition to one of the lower-energy electronic states driven by the solvent molecule, whose vibrational temperature was found to play a critical role in the process [110].

Wester *et al.* performed the only time-resolved investigation of a bimolecular S_N2 reaction in the gas phase by studying $I^- + CH_3I$ [111]. The reactants were derived from the precursor ion-dipole-bound cluster $I_2^- \cdot CH_3I$. The start trigger for the reaction is a femtosecond pump pulse, which dissociates the I_2^- chromophore. Upon its photodissociation, the neutral iodine leaves the cluster, while the S_N2 reactants I^- and CH_3I start to interact due to their charge–dipole interaction. A probe pulse creates a PES, which identifies reaction transients and products as a function of interaction time. In the experiment two different pump photon energies have been employed, which result in different kinetic energies of the I^- reactant. At $\lambda_{pump} = 790$ nm, this leads to a relative kinetic energy between I^- and CH_3I of 0.15 eV, where the interaction of CH_3I with I^- during dissociation has been neglected. The PES reveals that in this case the dominant process is the production of the vibrationally excited entrance channel complex $I^- \cdot CH_3I$ on a time-scale of 600 fs. In contrast, for $\lambda_{pump} = 395$ nm, the relative kinetic energy of the reactants I^- and CH_3I is 0.32 eV (see Figure 4). Contributions of $I^- \cdot CH_3I$ and I^- are now identified in the PES and can be separated. The complex contribution increases rapidly after the pump pulse with a time constant indistinguishable from the laser cross-correlation of 200 fs. Interestingly, it then shows an exponential decay on two different time-scales, which is mirrored in the I^- contribution. Since the reactants do not have sufficient energy to cross the central reaction barrier, this is interpreted as a decay of the complex back to reactants. The fast time constant was determined to be 0.75 ps, which compares to the vibrational period of the $I^- \cdots CH_3I$ stretching mode. It suggests fairly direct dissociation dynamics in which the I^- undergoes a quasi-elastic collision with CH_3I

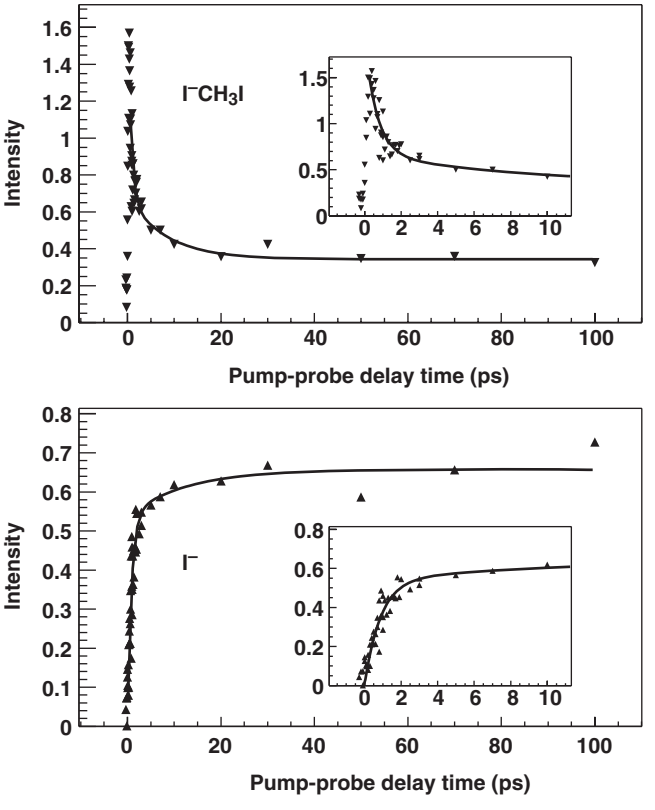

Figure 4. Signal intensity of I^-CH_3I (upper panel) and I^- (lower panel) in the femtosecond photoelectron spectra. Biexponential decay or growth curves, shown as solid lines, are found reproduce these signals [111].

before dissociation. The longer time constant of about 10 ps indicates that the complex is stabilized by energy flow from the reaction coordinate into the modes of the complex. It is comparable to the lifetime of the $Cl^- \cdot CH_3Cl$ entrance channel complex determined in the collisional stabilization experiments featured above.

5. Dynamics from differential scattering

In the previous sections we have discussed measurements of the total cross-section or the thermally averaged rate coefficient and illustrated how information on the reaction dynamics can be inferred from these measurements. A much more direct approach to the intrinsic dynamics of anion–molecule reactions is based on the measurement of the angle- and energy-differential scattering cross-section $d\sigma/d\Omega/dE$. For these experiments collisions of atoms and molecules with well-defined momentum vectors are prepared. Angle- and energy- or velocity-resolved detection schemes are employed to obtain the

differential cross-section. This approach of crossed-beam measurements of the differential scattering cross-section is widely used for neutral reactions [112,113]. We will discuss in the following two sections that it also proves to be valuable for anion–neutral reactions.

5.1. *Conventional crossed-beam reactive scattering*

The classical approach to crossed-beam reactive scattering is to cross two reactant beams at 90° and use a rotatable detector to measure the flux and the arrival time of products under a selected set of scattering angles in the laboratory frame of reference. From these laboratory flux data the differential cross-section in the centre-of-mass frame of the reaction is reconstructed, often using numerical simulations of the apparatus function. This approach has been developed for neutral-neutral reactions and has been used with great success to study the $F + H_2$ reaction (see e.g. [1]). In combination with the Rydberg tagging technique to measure the H atom product, the rotatable-detector setup is still the method of choice for this reaction [114].

The same detector concept has been applied to study elastic, inelastic and reactive channels in cation–molecule reactions (see Refs. [115,116] for reviews of the early work on cation–molecule reactive scattering). Here the main difference to neutral–neutral scattering experiments is, naturally, the production of the ion beam. Where the neutral beams are usually produced in supersonic expansions with a well-defined narrow range of velocities, the production of ion beams with a narrow velocity spread represents a major experimental challenge. For the study of chemical reactions the most interesting relative collision energies in the centre-of-mass frame range from millielectronvolts to a few electronvolts. Therefore ion beams have to be produced with a low kinetic energy and a correspondingly small energy spread. This was achieved for the first time in the 1970s for continuous beams of cations [117]. A high degree of control over the electric fields in the experimental setup, including contact potentials between different materials, is important to achieve a low energy spread. Even then, the Coulomb repulsion between the reactant ions in the beam ultimately limits the energy resolution for a given reactant density and thus scattering rate. For ion–molecule reactions this typically leads to a reduction in the ion reactant density by many orders of magnitude in comparison with a neutral supersonic beam. This is only to a small extent compensated by the higher detection efficiency for product ions in a charged-particle detector when compared to neutral products of neutral–neutral reactions which have to be ionized in the detector. Note that once control over the ion-beam energy is achieved in an experimental setup, the relative collision energy of the crossed beams can be continuously tuned by means of the ion acceleration potential. Such a tunable scattering energy is much more difficult to achieve for neutral–neutral reactions. There, different seed gases for the molecules in the supersonic beams and different intersection angles between the supersonic beams are required for the same purpose.

It was only in the 1990s that precise low-energy crossed-beam measurements with negative ions in a rotatable detector setup were carried out [116,118]. In the years before, the first detailed scattering experiments on anion–molecule reactions were carried out using a complex multiparticle coincidence scattering setup. With this setup reactions of heavy, mostly atomic, negative ions ($F^-, Cl^-, Br^-, I^-, S^-, CN^-$) with

lightweight hydrogen could be studied [119–122]. For example, for the $Cl^- + H_2$ collision, the kinematics of this combination have made it possible to study collisions down to 6 eV relative energy with an ion kinetic energies of 110 eV [119], which is significantly easier to handle experimentally than ion beams with only a few electronvolt kinetic energy. Furthermore, under these conditions the kinetic energy of the neutral product in the lab frame is large enough to be detected with a microchannel plate detector. With this technique the different channels for the collision of Cl^- with H_2, reactive proton transfer, forming $HCl + H^-$, reactive detachment, forming $HCl + H + e^-$, simple detachment, leading to $Cl + H_2 + e^-$, and dissociative detachment, leading to $Cl + H + H + e^-$, could be distinguished and their differential and absolute cross-sections could be measured as a function of the relative energy [119]. Also some information on the vibrational state population of the product molecule could be inferred. From these data the similarity of the dynamics of reactive proton transfer and reactive detachment could be deduced, where the branching between the two channels depends on the coupling to an intermediate autodetaching HCl^- state. Different scattering dynamics was found for the simple detachment channel, bearing a similarity with anion-rare gas collisions.

With the first crossed-beam measurements on anion–molecule reactions using low-energy ion sources and rotatable detectors, relative collision energies down to the millielectronvolt range and an energy resolution sufficient to resolve product vibrational states became accessible. In a benchmark experiment on the reaction of H^- with D_2, Zimmer and Linder determined the vibrational state-to-state differential and integral scattering cross-section [118,123]. The dominant forward scattering of the D^- product was attributed to a collinear reaction mechanism that requires scattering at small impact parameter. Wider angular distributions were observed for higher vibrational excitation of the HD product. From the measured product kinetic energy spectra also rotational state information could be extracted, studied in more detail for the inelastic scattering in $H^- + H_2$ collisions in the same laboratory [70].

Also in the 1990s, Farrar and coworkers started crossed-beam reactive scattering experiments of atomic oxygen with small closed-shell molecules, such as water, ammonia and hydrogen (see e.g. [116,125,126]). For the $O^- + H_2O$ reaction, which had already been studied before with crossed beams at higher collision energy and with lower resolution [127], they observed in the differential cross-section both a direct and an indirect reaction mechanism for the reactive channel of OH^- formation [125]. In addition they studied inelastic scattering via the $O^-(H_2O)$ reaction complex. More recently, non-reactive and reactive collisions of OH^- anions with D_2 molecules have been studied by the same group [124,128]. In the isotopic exchange reaction channel, the formation of $OD^- + HD$, no energy dependence was found between 0.27 and 0.69 eV relative collision energy [128]. In the measured narrow angular distribution it was found that the reaction occurs fast on the time-scale of rotation of the $OH^-(H_2)$ reaction complex. In a study of the proton transfer reaction channel, forming $HOD + D^-$, also a very narrow velocity distribution was extracted [124]. The reconstructed velocity distribution in the scattering plane is reproduced in Figure 5. These data also indicate a direct and fast reaction mechanism. The flux at smaller product ion velocities is caused by vibrational excitation of the bending mode in the HOD product. This can be attributed to a significant change of the water bond angle during the D^+ transfer.

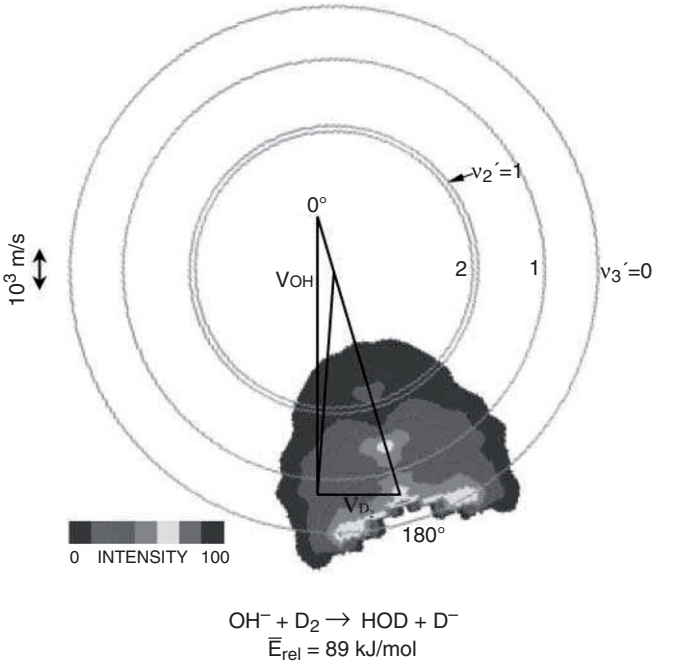

Figure 5. Newton diagram and extracted product flux contour map for the reaction $OH^- + D_2$ at 89 kJ/mol relative energy. The orthogonal black lines indicate the velocities of the incoming beams. The point in the centre of the circles represents the zero velocity in the centre-of-mass frame. Around this point the circles denote different product velocities. Smaller velocities indicate internal excitation of the HOD product molecule due to vibrational excitation of the bending mode (v_3) or the OD stretching mode (v_2). The measured flux shows that internal excitation, attributed to the bending mode of HOD, does occur during the reaction. Reprinted with permission from [124]. Copyright (2005), American Chemical Society.

5.2. *Velocity map imaging with crossed beams*

Compared to the conventional crossed-beam experiments with a rotatable detector, higher angular resolution and a much more rapid data acquisition is achieved with an imaging spectrometer. Moreover, such a spectrometer detects products irrespective of their velocity or scattering angle, i.e. it represents a detector with 4π solid angle of acceptance. Ion imaging has been combined with neutral reactive scattering starting with a study of the $H + D_2$ reaction [129] and is being successfully employed in a number of laboratories for reactive and inelastic crossed-beam scattering experiments [2,130–132]. The current spectrometers are based on the technique of velocity map imaging [133], which projects ions with the same velocity parallel to the detector surface onto the same spot on the detector. It thereby avoids broadening of the product ion images due to the finite size of the reaction volume.

To study ion–molecule reactions with crossed-beam imaging, we have constructed a velocity map imaging spectrometer and a versatile low-energy ion source [134]. This approach is in contrast with an early exploration of ion–molecule crossed-beam imaging, where *in situ* production of the reactant ions was used [135], an approach that is not

suitable for negative ions. In our experiment, slow ions with between 0.5 and 5 eV kinetic energy are brought to collision with neutral molecules in a supersonic molecular beam in the centre of the velocity map imaging electrode stack. Both reactant beams are pulsed to avoid a heavy gas load in the vacuum system. Once the two beams have crossed, the electric field of the imaging spectrometer is rapidly pulsed on and any product ions are projected onto the position-sensitive imaging detector. Ion impact positions, which are proportional to the velocity components in the scattering plane parallel to the detector surface, are recorded with a CCD camera. Recently, we improved the ion imaging electrodes to enhance the velocity resolution and we included a photomultiplier tube to measure the third, vertical, component of the product velocity vector [136].

With the ion–molecule crossed-beam imaging spectrometer we have studied the elementary S_N2-reaction of Cl^- with methyl iodide (CH_3I) at relative scattering energies between 0.4 and 2 eV [137]. The potential energy curve for this reaction along the reaction coordinate closely resembles Figure 1. As discussed already in Section 2 the characteristic deep potential minima, separated by an intermediate barrier, are found. In the reaction studied here this barrier lies submerged below the energy of the reactants. Nevertheless it strongly influences the reactivity in that the reaction occurs at only 10% of the Langevin or capture rate.

The imaging data, which is represented by an event list of impact velocity vectors in the laboratory frame, needs only little data processing. On the one hand, the transformation to the centre-of-mass frame has to be performed for each scattering event, which involves a translation and a rotation of the image parallel to the relative velocity vector. On the other hand, the loss of fast-moving reaction products needs to be corrected. Product ions with high laboratory velocities have a chance to leave the spectrometer volume that can be imaged onto the position-sensitive detector. This effect is referred to as 'density-to-flux correction' in neutral crossed-beam scattering experiments, where it also includes the correction for the spatial and velocity dependence of the ionization efficiency. For ion–molecule reactive imaging, the same correction function is used for all relative collision energies. It only depends on the magnitude of the laboratory velocity and not on its direction in the lab frame.

Two measured images of the differential cross-section in the centre-of-mass frame are shown in Figure 6 for two relative energies [137]. At 0.39 eV isotropic scattering of the I^- product ion is observed, indicative of an indirect reaction mechanism via a long-lived complex. Here, also much more energy is partitioned into internal excitation of the neutral CH_3Cl product. These are signatures of an indirect reaction mechanism with trapping of the collision partners in the minima of the intermolecular reaction potential. In contrast, at 1.9 eV the I^- ions scatter preferentially backward with respect to the direction of the incoming CH_3I. Also their velocity is found very near the maximum possible velocity. This is explained by a fast and direct reaction mechanism where the I^- leaves the reaction approximately collinearly with the incoming Cl^- anion.

In order to understand the details of the measured differential cross-sections theoretical calculation are employed. However, the theoretical description of polyatomic reactions that involve more than four atoms is very difficult. The present reaction involves six atoms and therefore twelve internal degrees of freedom. Such a large system cannot be calculated quantum mechanically and one has to resort to significant approximations. These are either quantum scattering calculations in reduced dimensions (typically four) [29] or

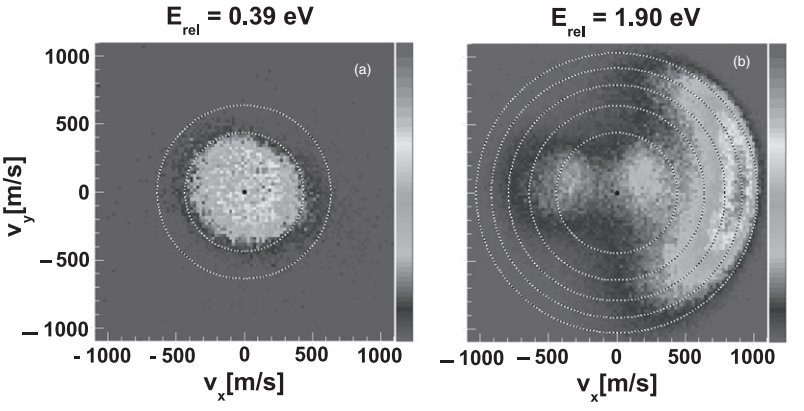

Figure 6. Measured differential scattering cross-section for the reaction of $Cl^- + CH_3I$ giving $ClCH_3 + I^-$. Shown are two images at 0.39 (left panel) and 1.9 eV (right panel) relative collision energy of the I^- velocity vector in the scattering plane obtained by velocity map slice imaging. The centre of each image denotes zero velocity in the centre-of-mass frame. The circles represent constant product velocities with the largest circle showing the maximum possible product velocity based on the known total energy in the reaction system. At 0.39 eV isotropic scattering is observed, indicative of an indirect reaction mechanism via a long-lived complex. At 1.9 eV most of the flux shows direct scattering with large product velocities (peak near $v_x \sim +1000$ m/s, but with about 10% probability, small product velocities both forward and backward scattered, are observed. These events are attributed to the indirect 'roundabout' mechanism (Taken from [137]).

calculations that treat the electronic structure quantum mechanically but propagate the nuclei classically on the Born–Oppenheimer surface [30].

Calculated trajectories show that at 1.9 eV collision energy a direct reaction mechanism governs the nucleophilic substitution reaction. The Cl^- ion moves into the umbrella of the hydrogen atoms and forms a bond with the central carbon atom. Roughly collinearly to this motion the I^- product ion is moving away after the three hydrogen atoms have inverted to form the $ClCH_3$ product molecule. This numerical results corresponds directly to the back-scattering observed in the experiment. The trajectory calculations also revealed another reaction mechanism that occurs with about 10% probability. In this mechanism the CH_3I reactant undergoes a single 360° revolution about an axis perpendicular to the C–I bond. Only after this revolution does the substitution occur. This mechanism, which we named the 'roundabout' mechanism, is found to go along with a large energy partitioning into internal degrees of freedom of the neutral product molecule. This agrees with the observed structures in the measured differential cross-sections at small I^- velocity (see Figure 6), which have therefore been attributed to the roundabout mechanism [137].

6. Perspectives

Negative ion reactions have been studied for a long time owing to their importance in many Earth-bound, planetary or astrophysical plasmas. In the last two decades research on the detailed dynamics of this class of reactions has flourished, owing to more and

more precise techniques to measure both integral and differential scattering studies. In this article we have presented an overview of these experimental approaches and how much they have taught us on the different, and sometimes peculiar, aspects of anion–molecule reaction dynamics.

We have shown that flow and drift tube measurements are well suited to study the thermal kinetics of anion–molecule reactions. At low temperature these studies are complemented and extended using cryogenic ion traps, which can also measure much smaller rate coefficients than drift tubes due to the long attainable interaction times. Guided ion beam experiments are ideal for precise measurements of integral cross-sections at well-defined relative energy over a large dynamic range. The dynamics of the transient reaction complex can be studied with direct time-resolved spectroscopy and its lifetime can also be indirectly inferred from ternary collision rates. When it comes to direct imaging of the full reaction dynamics, crossed-beam experiments are very revealing. In particular the new opportunities of crossed-beam velocity map ion imaging should be stressed here.

Despite a wealth of theoretical studies, detailed insight into the flow of energy via the coupling of different vibrational modes during the reaction continues to be inaccessible experimentally. Of particular interest is the regime of breakdown of ergodicity at the transition from a complex-mediated, statistical reaction mechanism to an impulsive, direct mechanism. It is in this range of relative collision energies, where crossed-beam imaging provides the best resolution. Reactive scattering with vibrationally excited reactants – as successfully used to shed light on chemical reactions of neutrals [132] – has not yet been explored for anion–molecule reactions. The role of non-reactive degrees of freedom in a reaction, referred to as the 'spectator modes', on the integral cross-section and the product branching is a matter of debate that needs answers from experiments. Reactive scattering with spatially aligned or oriented molecules would directly access the stereodynamics on the molecular level. Importantly, anion–molecule reactions have very different kinetics in solution. A bottom-up approach, introducing the solvent molecule per molecule in scattering experiments with microsolvated anions, would highlight the role of the environment on the dynamics. Questions about the role of quantum effects such as Feshbach scattering resonances, tunnelling, zero-point vibrational motion or decoherence free subspaces, can now be asked and demand innovative experimental approaches.

We expect that guided ion beam and ion trap studies as well as ion–molecule crossed-beam imaging will be most helpful to address some of these questions in the future. The combination of an ion trap as a source for internally cold molecular ions and clusters with a scattering experiment will allow for studies of the reactions of complex molecular systems while maintaining good control over their internal quantum states. Also merged ion and neutral beams represent a useful approach to study low-energy reactions, as demonstrated most recently for the reaction of H^- with H [138], which is considered to be important for the formation of H_2 in the early universe. Laser-cooling of the reactants may eventually provide even lower collision temperatures than buffer gas cooling, an approach that has been demonstrated for cation–neutral reactions [139]; Os^- is a possible candidate for anion laser-cooling [140,141]. All in all, there is also a lot of room for further research on anion–molecule reactions, which challenges the 'complexity limit' and ultimately allows us to understand and control all the subtleties of the chemical dynamics of multi-atom molecular systems.

Acknowledgements

We would like to thank our collaborators in the experiments on anion–molecule reaction dynamics, in particular Sebastian Trippel, Rico Otto, and Christoph Eichhorn. We also wish to thank Dan Neumark and Bill Hase for fruitful collaborations on reaction dynamics in general and nucleophilic substitution reactions in particular. Our research is supported by the Eliteförderung der Landesstiftung Baden-Württemberg, the Alexander von Humboldt Foundation, the Deutsche Forschungsgemeinschaft and the EU Marie Curie Initial Training Network ICONIC.

References

[1] Y. T. Lee, Angew. Chem. Int. Ed. Engl. **26**, 939 (1987).
[2] A. J. R. Heck and D. W. Chandler, Annu. Rev. Phys. Chem. **46**, 335 (1995).
[3] B. Whitaker, ed., *Imaging in Molecular Dynamics: Technology and Applications* (Cambridge University Press, Cambridge, UK, 2003).
[4] A. Sanov and R. Mabbs, Int. Rev. Phys. Chem. **27**, 53 (2008).
[5] A. Stolow, A. E. Bragg, and D. M. Neumark, Chem. Rev. **104**, 1719 (2004a).
[6] J. Doyle, B. Friedrich, R. V. Krems, and F. Masnou-Seeuws, Eur. Phys. J. D **31**, 149 (2004).
[7] R. Krems, Int. Rev. Phys. Chem. **24**, 99 (2005).
[8] P. B. Armentrout, Adv. At. Mol. Opt. Phys. **43**, 187 (2000a).
[9] D. Smith and P. Spanel, Mass Spectrom. Rev. **14**, 255 (1995).
[10] E. Herbst, Adv. Gas Phase Ion Chem. **3**, 1 (1998).
[11] S. Petrie and D. K. Bohme, Mass Spectrom. Rev. **26**, 258 (2007).
[12] M. C. McCarthy, C. A. Gottlieb, H. Gupta, and P. Thaddeus, Astrophys. J. Lett. **652**, L141 (2006).
[13] S. Brünken, H. Gupta, C. A. Gottlieb, M. C. McCarthy, and P. Thaddeus, Astrophys. J. Lett **664**, L43 (2007).
[14] C. H. DePuy, Int. J. Mass Spectrom. **200**, 79 (2000).
[15] S. Gronert, Chem. Rev. **101**, 329 (2001).
[16] K. M. Ervin, Chem. Rev. **101**, 391 (2001).
[17] R. D. Levine, *Molecular Reaction Dynamics* (Cambridge University Press, Cambridge, UK, 2005).
[18] N. I. Hammer, J. W. Shin, J. M. Headrick, E. G. Diken, J. R. Roscioli, G. H. Weddle, and M. A. Johnson, Science **306**, 675 (2004).
[19] D. M. Neumark, J. Phys. Chem. A **112**, 13287 (2008).
[20] X. B. Wang and L. S. Wang, Annu. Rev. Phys. Chem. **60**, 105 (2009).
[21] P. Hlavenka, R. Otto, S. Trippel, J. Mikosch, M. Weidemüller, and R. Wester, J. Chem. Phys. **130**, 061105 (2009).
[22] H. K. Gerardi, K. J. Breen, T. L. Guasco, G. H. Weddle, G. H. Gardenier, J. E. Laaser, and M. A. Johnson, J. Phys. Chem. A **114**, 1592 (2010).
[23] D. M. Neumark, Phys. Chem. Chem. Phys. **7**, 433 (2005).
[24] D. J. Pegg, Rep. Prog. Phys. **67**, 857 (2004).
[25] J. Simons, J. Phys. Chem. A **112**, 6401 (2008).
[26] R. Wester, in *Handbook of High Resolution Spectroscopy*, edited by M. Quack and F. Merkt (Wiley-Blackwell, Hoboken, NJ, 2010), chap. Spectroscopy and reaction dynamics of anions.
[27] D. C. Clary, Science **279**, 1879 (1998).
[28] S. C. Althorpe and D. C. Clary, Annu. Rev. Phys. Chem. **54**, 493 (2003).
[29] S. Schmatz, Chem. Phys. Chem. **5**, 600 (2004).
[30] W. L. Hase, Science **266**, 998 (1994).
[31] W. L. Hase, H. Wang, and G. H. Peslherbe, Adv. Gas Phase Ion Chem. **3**, 125 (1998).

[32] T. Su and M. T. Bowers, Int. J. Mass. Spectrom. Ion Physics **211**, 212 (1975).
[33] T. Su and W. J. Chesnavich, J. Chem. Phys. **76**, 5183 (1982).
[34] T. Su, J. Chem. Phys. **89**, 5355 (1988).
[35] K. F. Lim, Quant. Chem. Prog. Ex. **14**, 1 (1994).
[36] E. E. Ferguson, Annu. Rev. Phys. Chem. **26**, 17 (1975).
[37] E. E. Ferguson, Can. J. Chem. **47**, 1815 (1969).
[38] F. C. Fehsenfeld and E. E. Ferguson, J. Chem. Phys. **61**, 3181 (1974).
[39] C. H. DePuy and V. M. Bierbaum, Acc. Chem. Res. **14**, 146 (1981).
[40] W. Lindinger, A. Hansel, and A. Jordan, Int. J. Mass Spectrom. **173**, 191 (1998).
[41] A. A. Viggiano and S. Williams, Adv. Gas-Phase Ion Chem. **4**, 85 (2001).
[42] N. G. Adams and D. Smith, Int. J. Mass Spectrom. Ion Proc. **21**, 349 (1976).
[43] J. M. Vandoren, S. E. Barlow, C. H. Depuy, and V. M. Bierbaum, Int. J. Mass Spectrom. Ion Proc. **81**, 85 (1987).
[44] S. T. Arnold, J. V. Seeley, J. S. Williamson, P. L. Mundis, and A. A. Viggiano, J. Phys. Chem. A **104**, 5511 (2000).
[45] I. Korolov, T. Kotrik, R. Plasil, M. Hejduk, and J. Glosik, Contrib. Plas. Phys. **48**, 521 (2008).
[46] D. K. Böhme, Int. J. Mass Spectrom. **200**, 97 (2000).
[47] C. H. DePuy, S. Gronert, A. Mullin, and V. M. Bierbaum, J. Am. Chem. Soc. **112**, 8650 (1990).
[48] N. Eyet, S. M. Villano, and V. M. Bierbaum, J. Am. Soc. Mass Spectrom. **19**, 1296 (2008).
[49] S. M. Villano, N. Eyet, W. C. Lineberger, and V. M. Bierbaum, J. Am. Chem. Soc. **131**, 8227 (2009).
[50] J. V. Seeley, R. A. Morris, A. A. Viggiano, H. B. Wang, and W. L. Hase, J. Am. Chem. Soc. **119**, 577 (1997).
[51] I. S. K. Kerkines, K. Morokuma, N. Iordanova, and A. A. Viggiano, J. Chem. Phys. **132**, 044309 (2010).
[52] A. A. Viggiano, R. A. Morris, J. S. Paschkewitz, and J. F. Paulson, J. Am. Chem. Soc. **114**, 10477 (1992).
[53] J. K. Laehrdahl and E. Uggerud, Int. J. Mass Spectrom. **214**, 277 (2002).
[54] E. Uggerud, J. Phys. Org. Chem. **19**, 461 (2006).
[55] S. M. Villano, S. Kato, and V. M. Bierbaum, J. Am. Chem. Soc. **128**, 736 (2006).
[56] W. P. Hu and D. G. Truhlar, J. Am. Chem. Soc. **118**, 860 (1996).
[57] T. M. Miller, J. F. Friedman, J. S. Williamson, and A. A. Viggiano, J. Chem. Phys. **124**, 144305 (2006).
[58] P. B. Armentrout, Int. J. Mass Spectrom. **200**, 219 (2000b).
[59] E. Teloy and D. Gerlich, Chem. Phys. **4**, 417 (1974).
[60] D. Gerlich, Adv. Chem. Phys. **82**, 1 (1992).
[61] D. J. Levandier, R. A. Dressler, and E. Murad, Rev. Sci. Instrum. **68**, 64 (1997).
[62] V. F. DeTuri, P. A. Hintz, and K. M. Ervin, J. Phys. Chem. A **101**, 5969 (1997).
[63] E. Haufler, S. Schlemmer, and D. Gerlich, J. Phys. Chem. A **101**, 6441 (1997).
[64] D. Gerlich, J. Anal. At. Spec. **19**, 581 (2004).
[65] K. Rempala and K. M. Ervin, J. Chem. Phys. **112**, 4579 (2000).
[66] L. A. Angel and K. M. Ervin, J. Phys. Chem. A **105**, 4042 (2001).
[67] L. A. Angel, S. P. Garcia, and K. M. Ervin, J. Am. Chem. Soc. **124**, 336 (2002).
[68] F. A. Akin and K. M. Ervin, J. Phys. Chem. A **110**, 1342 (2006).
[69] L. A. Angel and K. M. Ervin, J. Am. Chem. Soc. **125**, 1014 (2003).
[70] H. Müller, P. Zimmer, and F. Linder, J. Phys. B **29**, 4165 (1996).
[71] S. E. Barlow, J. M. V. Doren, and V. M. Bierbaum, J. Am. Chem. Soc. **110**, 7240 (1988).
[72] L. Deng, V. Branchadell, and T. Ziegler, J. Am. Chem. Soc. **116**, 10645 (1994).
[73] M. N. Glukhovtsev, A. Pross, H. B. Schlegel, R. D. Bach, and L. Radom, J. Am. Chem. Soc. **118**, 11258 (1996).
[74] D. J. Mann and W. L. Hase, J. Phys. Chem. A **102**, 6208 (1998).

[75] G. Li and W. L. Hase, J. Am. Chem. Soc. **121**, 7124 (1999).
[76] C. Hennig and S. Schmatz, Phys. Chem. Chem. Phys. **7**, 1552 (2005).
[77] C. Hennig and S. Schmatz, J. Chem. Phys. **121**, 220 (2004).
[78] J. C. Polanyi, Acc. Chem. Res. **5**, 161 (1972).
[79] M. A. Smith, Int. Rev. Phys. Chem. **17**, 35 (1998).
[80] H. Zacharias, M. M. T. Loy, P. A. Roland, and A. S. Sudbo, J. Chem. Phys. **81**, 3148 (1984).
[81] A. E. Belikov, M. M. Ahern, and M. A. Smith, Chem. Phys. **234**, 195 (1998).
[82] M. Hawley and M. A. Smith, J. Chem. Phys. **95**, 8662 (1991).
[83] M. Hawley and M. A. Smith, J. Chem. Phys. **96**, 1121 (1992).
[84] J. L. Le Garrec, B. R. Rowe, J. L. Queffelec, J. B. A. Mitchell, and D. C. Clary, J. Chem. Phys. **107**, 1021 (1997).
[85] D. Gerlich, Phys. Scripta **T59**, 256 (1995).
[86] R. Wester, J. Phys. B **42**, 154001 (2009).
[87] R. Otto, J. Mikosch, S. Trippel, M. Weidemüller, and R. Wester, Phys. Rev. Lett. **101**, 063201 (2008).
[88] D. K. Bohme, R. S. Hemsworth, and H. W. Rundle, J. Chem. Phys. **59**, 77 (1973).
[89] J. Troe, J. Chem. Soc. Far. Trans. **90**, 2303 (1994).
[90] C. Li, P. Ross, J. E. Szulejko, and T. B. McMahon, J. Am. Chem. Soc. **118**, 9360 (1996).
[91] J. Mikosch, R. Otto, S. Trippel, C. Eichhorn, M. Weidemüller, and R. Wester, J. Phys. Chem. A **112**, 10448 (2008a).
[92] S. T. Graul and M. T. Bowers, J. Am. Chem. Soc. **113**, 9696 (1991).
[93] S. T. Graul and M. T. Bowers, J. Am. Chem. Soc. **116**, 3875 (1994).
[94] S. T. Graul, C. J. Carpenter, J. E. Bushnell, P. A. M. van Koppen, and M. T. Bowers, J. Am. Chem. Soc. **120**, 6785 (1998).
[95] H. Wang, G. H. Peslherbe, and W. L. Hase, J. Am. Chem. Soc. **116**, 9644 (1994).
[96] S. L. Craig, M. Zhong, and J. I. Brauman, J. Am. Chem. Soc. **121**, 11790 (1999).
[97] D. S. Tonner and T. B. McMahon, J. Am. Chem. Soc. **122**, 8783 (2000).
[98] P. Ayotte, J. Kim, J. A. Kelley, S. B. Nielsen, and M. A. Johnson, J. Am. Chem. Soc. **121**, 6950 (1999).
[99] S. L. Craig, M. Zhong, and J. I. Brauman, J. Am. Chem. Soc. **120**, 12125 (1998).
[100] N. F. Scherer, C. Sipes, R. B. Bernstein, and A. H. Zewail, J. Chem. Phys. **92**, 5239 (1990).
[101] J. C. Williamson, J. M. Cao, H. Ihee, H. F. H, and A. H. Zewail, Nature **386**, 159 (1997).
[102] A. Stolow, A. E. Bragg, and D. M. Neumark, Chem. Rev. **104**, 1719 (2004b).
[103] A. Stolow and J. G. Underwood, Adv. Chem. Phys. **139**, 497 (2008).
[104] R. Mabbs, E. R. Grumbling, K. Pichugin, and A. Sanov, Chem. Soc. Rev. **38**, 2169 (2009).
[105] B. J. Greenblatt, M. T. Zanni, and D. M. Neumark, Chem. Phys. Lett. **258**, 523 (1996).
[106] M. T. Zanni, V. S. Batista, B. J. Greenblatt, W. H. Miller, and D. M. Neumark, J. Chem. Phys. **110**, 3748 (1999).
[107] A. V. Davis, R. Wester, A. E. Bragg, and D. M. Neumark, J. Chem. Phys. **118**, 999 (2003).
[108] R. Mabbs, K. Pichugin, and A. Sanov, J. Chem. Phys. **122**, 054308 (2005).
[109] T. Sanford, S. Y. Han, M. A. Thompson, R. Parson, and W. C. Lineberger, J. Chem. Phys. **122**, 054307 (2005).
[110] L. Sheps, E. M. Miller, S. Horvath, M. A. Thompson, R. Parson, A. B. McCoy, and W. C. Lineberger, Science **328**, 220 (2010).
[111] R. Wester, A. E. Bragg, A. V. Davis, and D. M. Neumark, J. Chem. Phys. **119**, 10032 (2003).
[112] P. Casavecchia, Rep. Prog. Phys. **63**, 355 (2000).
[113] K. Liu, Annu. Rev. Phys. Chem. **52**, 139 (2001).
[114] M. Qiu, Z. Ren, L. Che, D. Dai, S. A. Harich, X. Wang, X. Yang, C. Xu, D. Xie, M. Gustafsson, *et al.*, Science **311**, 1440 (2006).
[115] J. H. Futrell, Adv. Chem. Phys. **82**, 501 (1992).
[116] J. M. Farrar, Annu. Rev. Phys. Chem. **46**, 525 (1995).

[117] M. L. Vestal, C. R. Blakley, P. W. Ryan, and J. H. Futrell, Rev. Sci. Instrum. **47**, 15 (1976).
[118] M. Zimmer and F. Linder, J. Phys. B **28**, 2671 (1995).
[119] M. Barat, J. C. Brenot, J. A. Fayeton, J. C. Houver, J. B. Ozenne, R. S. Berry, and M. Durup-Ferguson, Chem. Phys. **97**, 165 (1985).
[120] J. A. Fayeton, J. C. Brenot, M. Durup-Ferguson, and M. Barat, Chem. Phys. **133**, 259 (1989).
[121] J. C. Brenot, M. Durupferguson, J. A. Fayeton, K. Goudjil, and M. Barat, Chem. Phys. **179**, 557 (1994).
[122] K. Goudjil, J. C. Brenot, M. Durup-Ferguson, and J. Fayeton, Chem. Phys. **179**, 573 (1994).
[123] M. Zimmer and F. Linder, Chem. Phys. Lett. **195**, 153 (1992).
[124] Li, S. T. Lee, and J. M. Farrar, J. Phys. Chem. A **109**, 6392 (2005).
[125] D. F. Varley, D. J. Levandier, and J. M. Farrar, J. Chem. Phys. **96**, 8806 (1992).
[126] D. J. Levandier, D. F. Varley, and J. M. Farrar, J. Chem. Phys. **97**, 4008 (1992).
[127] M. P. Karnett and R. J. Cross, Chem. Phys. Lett. **82**, 277 (1981).
[128] S. T. Lee and J. M. Farrar, J. Chem. Phys. **113**, 581 (2000).
[129] T. N. Kitsopoulos, M. A. Buntine, D. P. Baldwin, R. N. Zare, and D. W. Chandler, Science **260**, 1605 (1993).
[130] M. S. Elioff, J. J. Valentini, and D. W. Chandler, Science **302**, 1940 (2003).
[131] J. J. Lin, J. Zhou, W. Shiu, and K. Liu, Science **300**, 966 (2003).
[132] W. Zhang, H. Kawamata, and K. Liu, Science **325**, 303 (2009).
[133] A. T. J. B. Eppink and D. H. Parker, Rev. Sci. Instrum. **68**, 3477 (1997).
[134] J. Mikosch, U. Frühling, S. Trippel, D. Schwalm, M. Weidemüller, and R. Wester, Phys. Chem. Chem. Phys. **8**, 2990 (2006).
[135] E. L. Reichert, G. Thurau, and J. C. Weishaar, J. Chem. Phys. **117**, 653 (2002).
[136] S. Trippel, M. Stei, R. Otto, P. Hlavenka, J. Mikosch, C. Eichhorn, U. Lourderarj, J. X. Zhang, W. L. Hase, M. Weidemüller, *et al.*, J. Phys. Conf. Series **194**, 012046 (2009).
[137] J. Mikosch, S. Trippel, C. Eichhorn, R. Otto, U. Lourderaj, J. X. Zhang, W. L. Hase, M. Weidemüller, and R. Wester, Science **319**, 183 (2008b).
[138] H. Bruhns, H. Kreckel, K. Miller, M. Lestinsky, B. Seredyuk, W. Mitthumsiri, B. L. Schmitt, M. Schnell, X. Urbain, M. L. Rappaport, *et al.*, Rev. Sci. Instrum. **81**, 013112 (2010).
[139] S. Willitsch, M. T. Bell, A. D. Gingell, and T. P. Softley, Phys. Chem. Chem. Phys. **10**, 7200 (2008).
[140] R. C. Bilodeau and H. K. Haugen, Phys. Rev. Lett. **85**, 534 (2000).
[141] U. Warring, M. Amoretti, C. Canali, A. Fischer, R. Heyne, J. O. Meier, C. Morhard, and A. Kellerbauer, Phys. Rev. Lett. **102**, 043001 (2009).